Insights into the slow-onset tight-binding inhibition of *Escherichia coli* Dihydrofolate Reductase: detailed mechanistic characterization of Pyrrolo [3,2-f] quinazoline-1, 3-diamine and its derivatives as novel tight-binding inhibitors

Bharath Srinivasan[a,b] and Jeffrey Skolnick [a,d]

[a]Center for the Study of Systems Biology, School of Biology, Georgia Institute of Technology, 250, 14th Street, N.W., Atlanta, Georgia 30318, United States.

[b] bharath.srinivasan@biology.gatech.edu, [c]

[d] Corresponding author, skolnick@gatech.edu, Tel: (404) 407-8975, Fax: (404) 385-7478

SUPPORTING INFORMATION

Table S1. Kinetic parameters for *E. coli* DHFR*[,#]

S.No.	Substrate/ cofactor	K_m (μM)	V_{max} (μmol min^{-1} mg^{-1})	k_{cat} (sec^{-1})	k_{cat}/K_m ($sec^{-1}\mu M^{-1}$)
1.	Dihydrofolic acid	2.6 ± 0.5	60.9 ± 2.3	18.28 ± 0.70	7.03 ± 0.28
2.	NADPH	3.3 ± 0.5	59.6 ± 2.1	17.88 ± 0.63	5.42 ± 0.19

* The assays were performed at room temperature (at ~ 22 °C) and pH 7.3; [#] the values match, within experimental error, to values reported in literature[1, 2].

References:

1. Murakami, C., Ohmae, E., Tate, S., Gekko, K., Nakasone, K. & Kato, C. (2010) Cloning and characterization of dihydrofolate reductases from deep-sea bacteria, *Journal of biochemistry.* **147**, 591-9.
2. Stone, S. R. & Morrison, J. F. (1988) Dihydrofolate reductase from Escherichia coli: the kinetic mechanism with NADPH and reduced acetylpyridine adenine dinucleotide phosphate as substrates, *Biochemistry.* **27**, 5493-9.
3. Notredame, C., Higgins, D. G. & Heringa, J. (2000) T-Coffee: A novel method for fast and accurate multiple sequence alignment, *Journal of molecular biology.* **302**, 205-17.
4. Gouet, P., Courcelle, E., Stuart, D. I. & Metoz, F. (1999) ESPript: analysis of multiple sequence alignments in PostScript, *Bioinformatics.* **15**, 305-8.
5. Guex, N. & Peitsch, M. C. (1997) SWISS-MODEL and the Swiss-PdbViewer: an environment for comparative protein modeling, *Electrophoresis.* **18**, 2714-23.

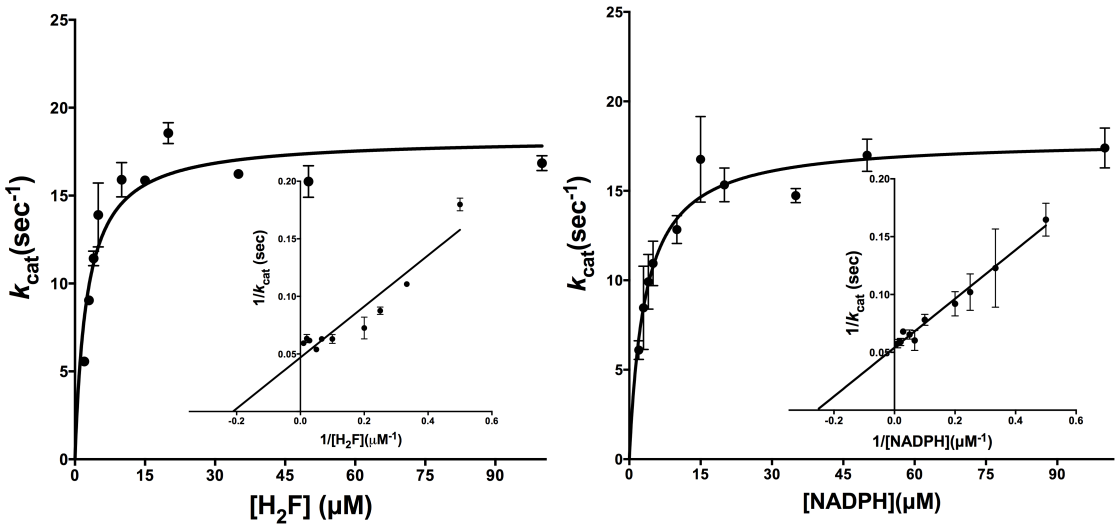

Fig S1. Kinetic parameters of *E. coli* DHFR for its substrates **A)** H_2F and **B)** NADPH. The experimental data points are fit to the Michaelis-Menten equation using the non-linear curve fitting algorithms of GraphPad Prism v 6.0e. Inset shows the double-reciprocal LB plot for the respective curves.

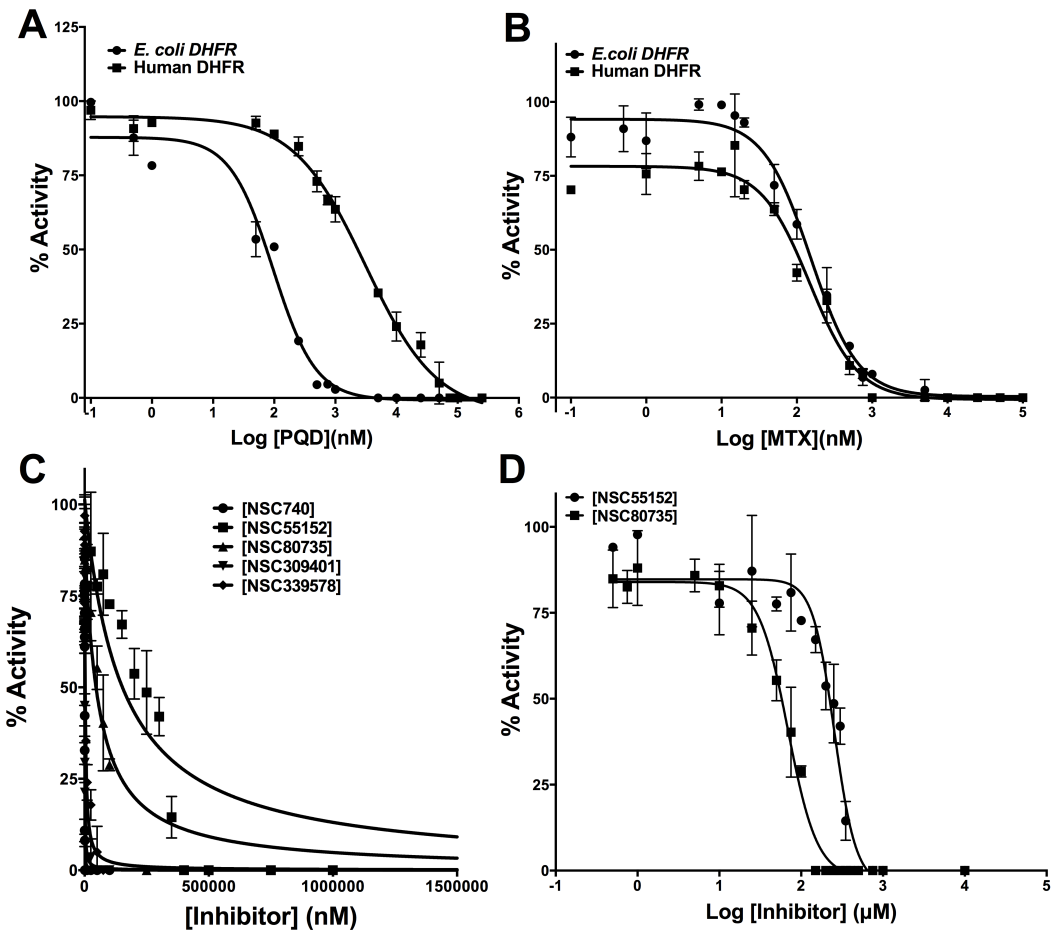

Fig S2. Curves to determine the IC-50 values for a select set of small molecules identified in our study. **A)** IC-50 values for PQD (NSC339578) determined for *E. coli* and human DHFR and **B)** IC-50 values for MTX (NSC740) determined for *E. coli* and human DHFR. **C)** Fit of the experimental dose-response curves to Morrison's tight-binding equation for inhibitors of human DHFR. **D)** IC-50 value estimates for inhibitors of human DHFR not displaying tight-binding behavior (NSC80735 and NSC55152). On the plots, the y-axis represents % activity of the enzyme and the x-axis represents the log inhibitor concentration/inhibitor concentration. The experimental data points were fit to the respective equations using the non-linear curve-fitting algorithm of GraphPad Prism v 6.0e.

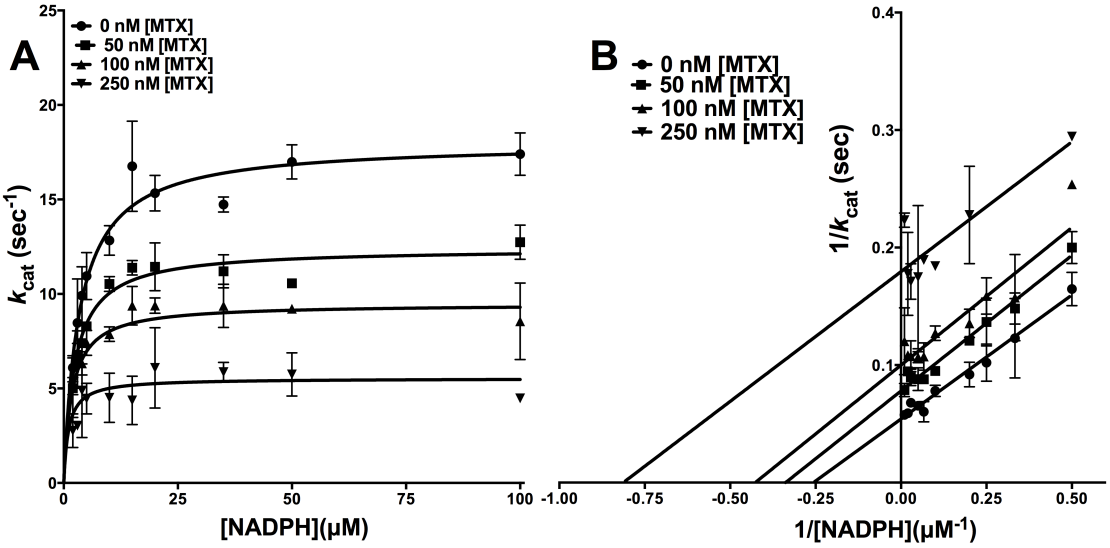

Fig S3. MTX-NADPH inhibition kinetics for *E. coli* DHFR **A)** Fit of the primary data to the uncompetitive inhibition model for NADPH titration at several fixed concentrations of MTX (NSC740) for *E. coli* DHFR, **B)** Double reciprocal Lineweaver-Burk plot of NADPH titration at several fixed concentrations of MTX for *E. coli* DHFR.

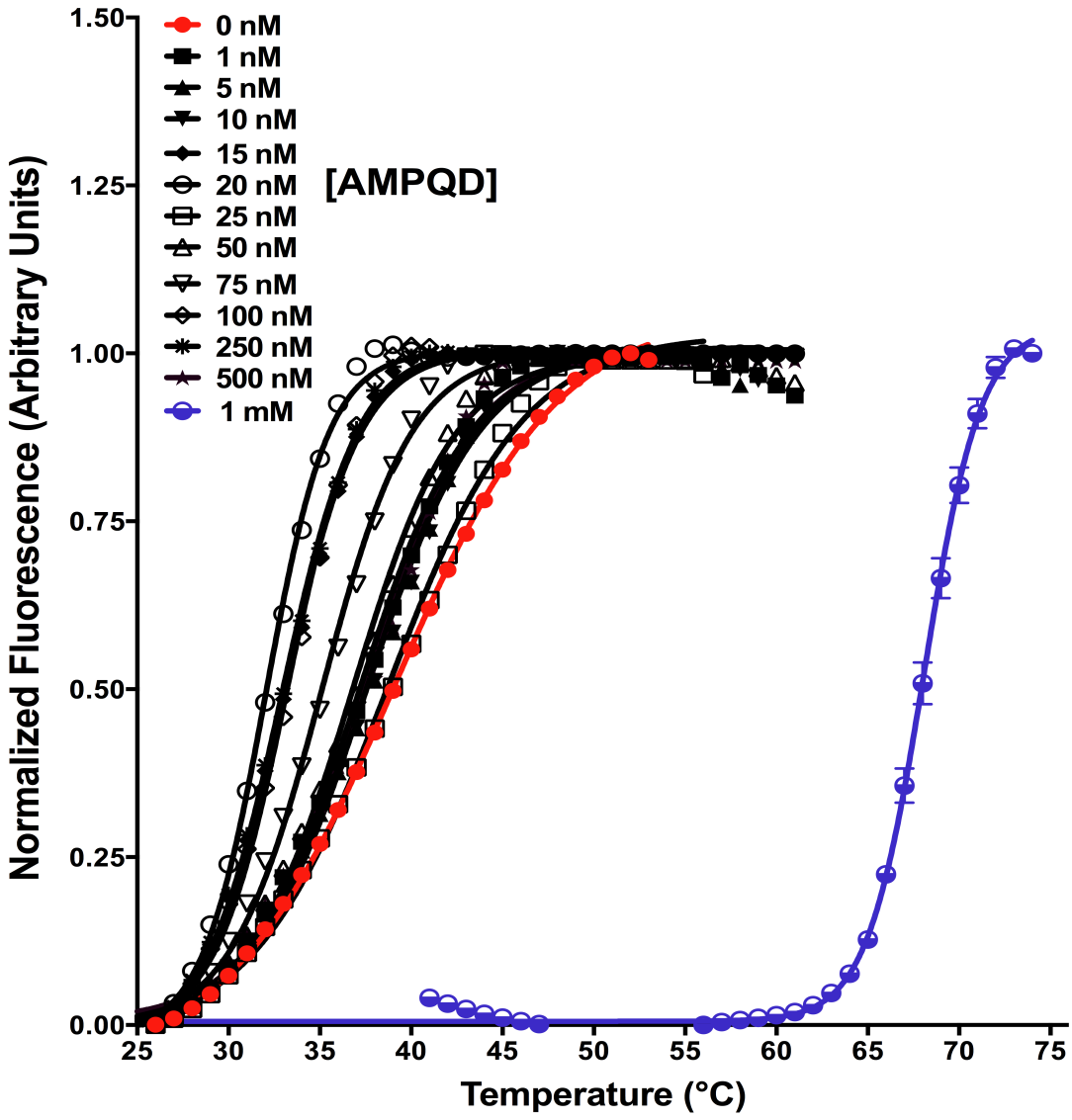

Fig S4. Thermal shift assay curves for *E. coli* DHFR at varying concentrations of the inhibitor AMPQD. The inhibitor was titrated from 0 nM-500 nM. The protein alone curve is shown in red color while the protein melting curve in the presence of 1 mM AMPQD is shown in blue.

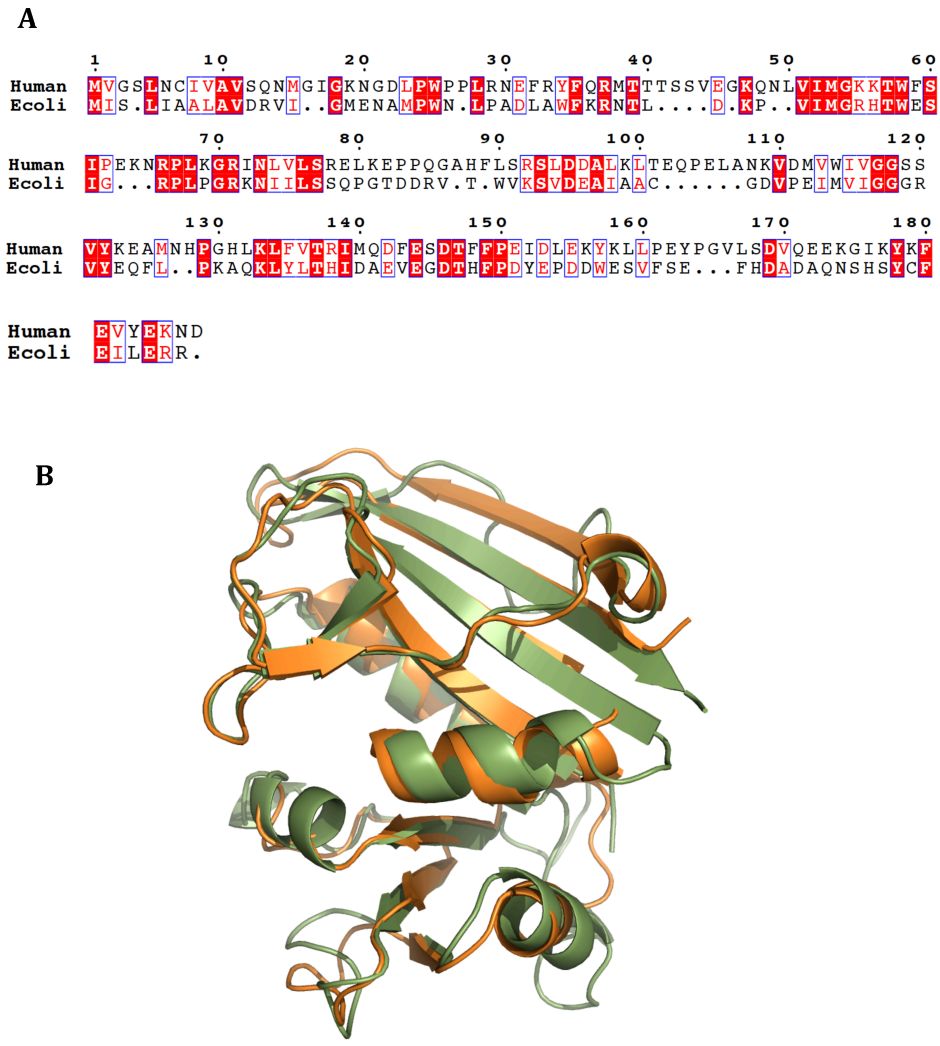

Fig S5. Comparison between *E. coli* and human DHFR **A)** Sequence alignment between the sequences of *E. coli* and human DHFRs. The alignment was generated with T-COFFEE [3], and the figure was generated with ESpript [4]. **B)** Structural alignment of human DHFR (PDB ID: 4G95) (orange color) and *E. coli* DHFR (PDB ID: 4P66) (green color). The alignment was generated in SPDBV [5] and the figure was rendered in MacPyMOL.

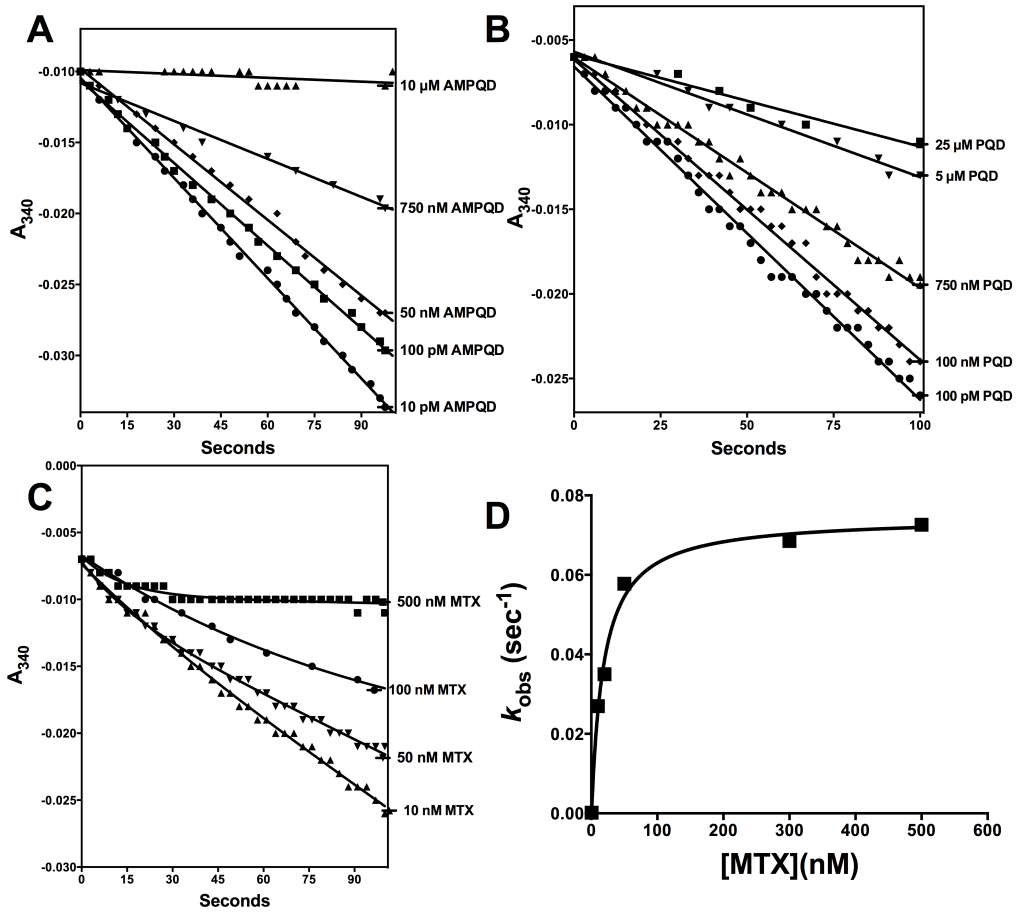

Fig S6. Time course analysis for human DHFR inhibition. **(*A*)** Time-dependent inactivation of human DHFR by 10 pM–10 µM AMPQD. **(B)** Time-dependent inactivation of human DHFR by 100 pM–25 µM PQD. **(C)** Time-dependent inactivation of human DHFR by 10 nM–500 nM MTX. **D)** Plot of k_{obs} (obtained by fit of curves in panel (C) to equation 7) vs. MTX concentration. The curve was fit to equation 8 (see materials and methods). For panel (A), (B) and (C), x-axis represents the time in seconds, and the y-axis shows the rate of conversion of NADPH to NADP monitored at 340 nm. The symbols represent the experimental data points and the solid curves represent the best fit of the data to Eq. 7 for slow binding inhibition using GraphPad Prism v 6.0e.

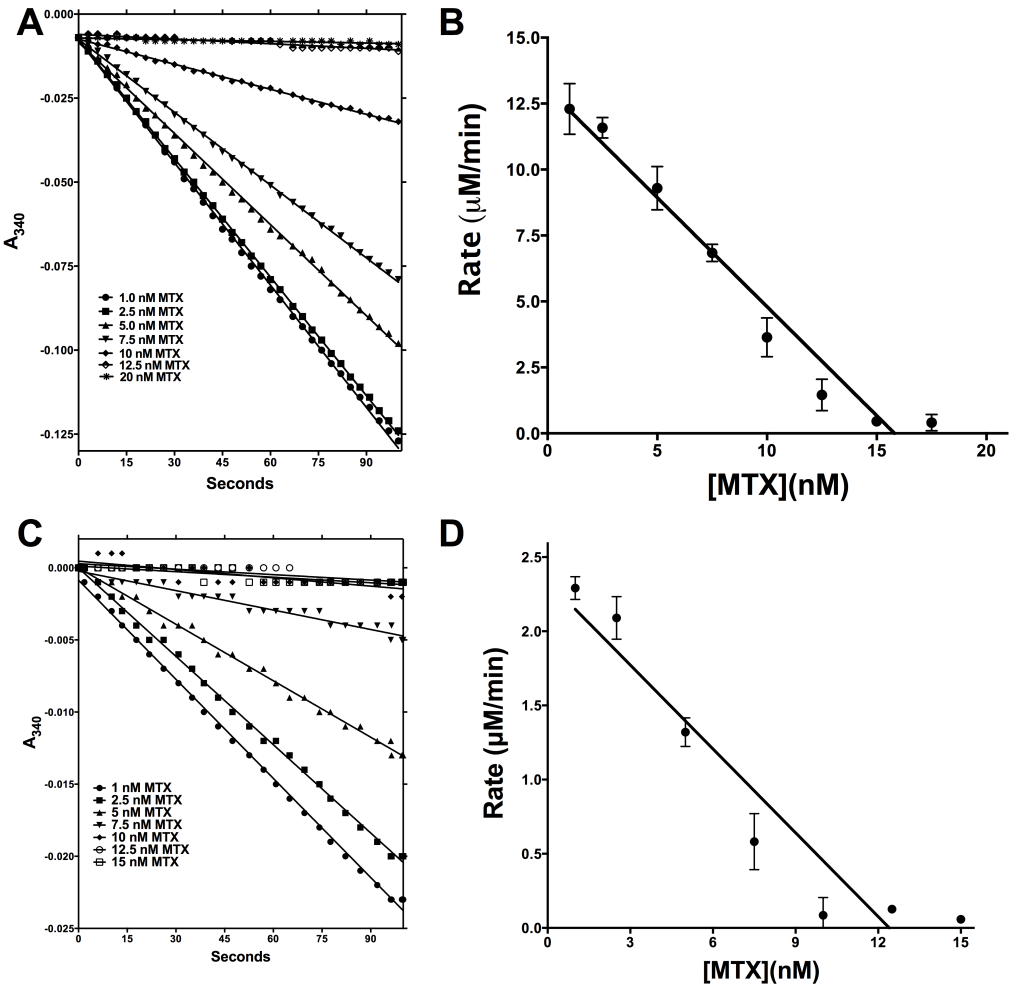

Fig S7. Enzyme concentration estimation by the velocity-titration curve method. **(A)** Time-dependence of inactivation of *E. coli* DHFR after preincubating the enzyme with varying concentrations of MTX for 300 seconds. **B)** Replot of the rate of formation of NADP vs. MTX concentration to obtain an estimate of the catalytically active enzyme concentration for *E. coli* DHFR. **C)** Time-dependence of inactivation of human DHFR after preincubating the enzyme with varying concentrations of MTX for 300 seconds. **D)** Replot of the rate of formation of NADP vs. MTX concentration to obtain an estimate of the catalytically active enzyme concentration for human DHFR. The x-axis intercept indicates the molar concentration of enzyme present.